Construction of Highly Ordered Lamellar Nanostructures through Langmuir–Blodgett Deposition of Molecularly Thin Titania Nanosheets Tens of Micrometers Wide and Their Excellent Dielectric Properties

Kosho Akatsuka,[†,‡] Masa-aki Haga,[§,*] Yasuo Ebina,[†] Minoru Osada,[†] Katsutoshi Fukuda,[†] and Takayoshi Sasaki[†,‡,*]

[†]International Center for Materials Nanoarchitectonics, National Institute for Materials Science, 1-1 Namiki, Tsukuba, Ibaraki 305-0044, Japan, [‡]Graduate School of Pure and Applied Sciences, University of Tsukuba, 1-1-1 Tennodai, Tsukuba, Ibaraki 305-8571, Japan, and [§]Department of Applied Chemistry, Faculty of Science and Engineering, Chuo University, 1-13-27 Kasuga, Bunkyo-ku, Tokyo 112-8551, Japan

ABSTRACT Exfoliated unilamellar titania nanosheets of $Ti_{0.87}O_2$ with a lateral size of 10–30 μm were deposited layer-by-layer onto various substrates by Langmuir–Blodgett procedure to produce a highly ordered lamellar nanofilms. The nanosheets dispersed in an aqueous suspension containing quaternary ammonium ions as a supporting electrolyte floated spontaneously at the air/liquid interface, and they were successfully transferred onto the substrate after surface compression. Neat tiling of the nanosheets could be realized at an optimized surface pressure. The film thus obtained was exposed to UV light to turn the substrate surface hydrophilic, which was helpful for stable repetition of monolayer deposition. Layer-by-layer growth was confirmed by UV–visible absorption spectra, which showed progressive enhancement of an absorption band due to the nanosheet. Cross-sectional transmission electron microscopy images visualized the ultrathin film homogeneously deposited on the substrate surface and a lamellar fringe of the layer-by-layer assembled nanosheets was clearly resolved at a higher magnification. X-ray diffraction data on the films showed sharp basal reflections up to the seventh order, and Williamson–Hall analysis of the pattern indicated that the film was coherent across the total thickness with respect to X-ray and that the lattice strain was extremely small. In addition, the first basal reflection was accompanied by small satellite peaks, which are accounted for by the Laue interference function. All these features clearly indicate the formation of a highly ordered lamellar nanostructure of the titania nanosheets comparable to artificial lattice films produced via modern vapor-phase deposition processes. The obtained films showed superior dielectric and insulating properties as a reflection of the highly organized film nanoarchitecture.

KEYWORDS: nanosheet · Langmuir–Blodgett procedure · layer-by-layer deposition · multilayer film · dielectric properties

The organization of nanoscale materials as a building block has become a very important topic because the development of nanodevices with sophisticated functions is expected through this approach.[1–6] Among a number of nanomaterials of various size, shape, and structure, inorganic nanosheets derived from layered host compounds via soft-chemical delamination are one of the most suitable building blocks for designing films with a well-controlled nanostructure. The nanosheets correspond to a single layer, or a fundamental unit of layered structure. Accordingly their thickness is extremely small, 0.5–3 nm, being dependent on original layered material.[7–10] In contrast, the lateral dimensions are much larger, generally over a thousand times larger than the thickness, resulting in very high two-dimensional (2D) anisotropy. These structural features are comparable to atomic layers manipulated as a deposition unit in beam epitaxy techniques.

Up until now, a range of layered materials has been successfully delaminated to produce a rich library of nanosheets.[7–17] Furthermore, it has been clarified that these nanosheets exhibit various physical properties, depending on their composition and structure. For example, Ti or Nb-based oxide nanosheets, $Ti_{1-\delta}O_2$ and $Ca_2Nb_3O_{10}$ as typical members, show excellent photochemical and dielectric properties.[18,19] Room-temperature ferromagnetic and photoluminescent properties have been attained by incorporating magnetic elements (Co or Fe) and lanthanide elements (Eu, Tb···),[20–28] respectively, into these 2D nanosheet packages. In addition, MnO_2 and $Cs_4W_{11}O_{36}$ nanosheets undergo a reversible electrochemical redox reaction and photochromic process, respectively.[29,30]

© 2009 American Chemical Society

Several groups have demonstrated layer-by-layer deposition of nanosheets into a multilayer system *via* sequential adsorption through electrostatic self-assembly with oppositely charged polyelectrolytes.[31−37] Various useful functionalities, such as energy conversion,[38−42] magneto-optical response,[20−22] and molecular recognition,[43] have been realized through the design of multilayer films using nanosheets as a functional module. Film architecture can be, in principle, controlled at 1−2 nm steps, or the nanosheet thickness, along the film normal. This controllability is far superior to that of conventional wet-processes such as the sol−gel method and is comparable to that of modern vapor-phase deposition techniques. However, the quality, or structural integrity, of the reported nanosheet films was not satisfactory, being much poorer compared with artificial lattice films constructed by beam epitaxy techniques. This is not favorable for some emerging applications of nanosheet films, for example, as high-*k* nanofilms and as a seed layer for oriented growth of functional crystal films.[19,44] One of the main reasons for this deteriorated quality is based on random adsorption of 2D nanosheets with a finite lateral size of several hundred nanometers onto the oppositely charged substrate surface.[35,37] Most nanosheets are generally in such lateral dimensions because they are derived from the powder polycrystalline sample of the starting layered compound. Overlaps and gaps between the nanosheets are inevitably formed at high density in a single step of nanosheet deposition. Repeated deposition will intensify the disordered arrangement, leading to a multilayer structure of poor quality.

The lateral size of nanosheets is dependent on the crystal size of the starting layered compound and the strength of mechanical shear applied in the delamination process. Accordingly large-sized nanosheets up to several tens of micrometers can be obtained under favorable conditions.[15,45] We have demonstrated that sequential adsorption of oversized titania nanosheet, $Ti_{0.87}O_2$, and application of ultrasonic wave could yield a fairly well-ordered multilayer film.[46] Ultrasonication at an optimized power removed overlapped patches to produce a monolayer film in which nanosheets were densely tiled having a nearly negligible overlap area between them. The mean surface roughness was suppressed to around 0.3 nm in such film and sharp basal X-ray diffraction (XRD) peaks evolved from the multilayer structure.

Langmuir−Blodgett (LB) deposition has been proved effective as another approach for organizing 2D nanosheets.[47−55] The pioneering work by two groups demonstrated that clay organocomplexes could be spread on aqueous phase and transferred to a substrate.[47,48] Subsequent studies showed that exfoliated nanosheets of aluminosilicate (clay minerals),[49] layered molybdenum disulfide,[50] and layered titanate could float by adhering to amphiphilic ammonium cat-
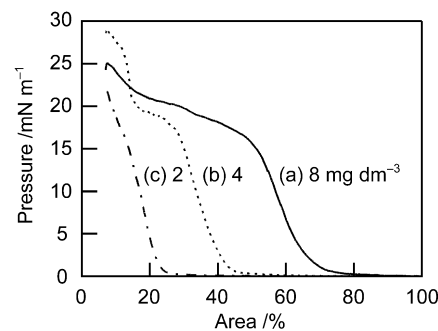
Figure 1. Pressure−area ($\pi-A$) isotherms for $Ti_{0.87}O_2$ nanosheet suspension at a concentration of (a) 8, (b) 4, and (c) 2 mg dm^{-3} at 25 °C. For the abscissa axis, the percentage of surface area relative to the area before compression is used instead of the molecular area, commonly employed, because the nanosheets inevitably show size distribution in the range of 10−30 μm.

ions at the interface through electrostatic interaction, and thus ordinary LB procedure was successfully applied to fabricate nanosheet films. The resulting films are characterized by neat-tiling arrangements of nanosheets without considerable gaps and overlaps. Such high-quality film architecture is attained *via* compression of the air/liquid interface prior to film transfer to a substrate, which should promote the lateral packing of nanosheets. However, when repeating the LB transfer to yield a multilayer structure, its stacking order is not, in general, very high compared with artificial lattice films. The nanosheet size smaller than 1 μm would be responsible for these unsatisfactory results.

We expect that LB deposition of nanosheets several tens of micrometers wide dramatically improve the film quality. Such large nanosheets have a lateral area >10000 times larger than that of nanosheets used in previous studies above,[54] which means the occurrence of sheet boundaries or defects should be suppressed to a level of <1/10000 times smaller. Successful deposition could produce a lamellar lattice comparable to films tailored by vapor-phase deposition, which will open promising application fields of nanosheets. Layer-by-layer assembly of such oversized nanosheets is, however, a great challenge due to such anticipated difficulties as floating and laterally organizing large 2D entities at the air/liquid interface as well as transferring them intact onto a substrate. No work has been reported because of these reasons and limited availability of oversized nanosheets. In the present study, multilayer buildup of large titania nanosheets (10−30 μm) *via* LB technique was examined. High structural order was realized as demonstrated through analysis of XRD data and transmission electron microscopy (TEM) observation.

RESULTS AND DISCUSSION

Pressure−Area ($\pi-A$) Isotherms of $Ti_{0.87}O_2$ Nanosheet Floating at the Suspension Surface. Figure 1 shows $\pi-A$ isotherms at 25 °C for colloidal suspensions at different

content of $Ti_{0.87}O_2$ nanosheet. A rise in surface pressure was observed without spreading amphiphilic additives as a general practice in the LB procedure. The same phenomenon was observed for the colloidal suspension of a smaller $Ti_{0.91}O_2$ nanosheet of ~300 nm. This behavior can be ascribed to the moderate amphiphilic nature of tetrabutyl-ammonium (hereafter TBA) ions used as a delaminating agent.[54] TBA ions trapped at the air/liquid interface interact with the negatively charged nanosheets and cause them to float. The present result is surprising in that much heavier nanosheets (about 10000 times larger in lateral dimensions and consequently 10000 times heavier) can float at the air/liquid interface. We still recognized, however, that the oversized nanosheet at the interface has a tendency to sink with time. In the LB deposition process, some duration is needed to obtain a saturated population of floating nanosheets after placing the suspension in the LB trough.[56] For the smaller nanosheet of $Ti_{0.91}O_2$, the floating fraction became larger with time and stayed nearly constant at 30 min and longer. In contrast, the number of floating oversized nanosheets reached a maximum at 20 min and declined afterward. Thus we employed a shorter time of 20 min in the present LB deposition.

The lift-off area of $\pi-A$ isotherms shifted to the larger area side with increasing the $Ti_{0.87}O_2$ nanosheet concentration from 2 to 8 mg dm^{-3}. This tendency is reflected in the number of nanosheets floating at the surface, which should be directly related to the nanosheet concentration in the suspension. The isotherm curves showed an inflection point at a surface pressure of ~16 mN m^{-1}. The pressure increased steeply up to the inflection point and a rather gradual slope region appeared at the higher pressure. This behavior should be related to how the floating nanosheets are organized at the air/liquid interface, which can be examined by atomic force microscope (AFM) observations of the nanosheet films transferred onto a silicon wafer substrate at various pressures. In the film transferred from the suspension of 8 mg dm^{-3} at a low surface pressure of <3 mN m^{-1}, the nanosheets were loosely packed with noticeable gaps between them (Figure 2a). A height histogram from this image clearly indicates the presence of the gap, giving a small peak at −1.3 nm. Note that the prominent peak taken at 0 nm denotes the nanosheets transferred onto the substrate in a monolayer. The difference of 1.3 nm between the major peak and the small one corresponds to the nanosheet thickness (see Supporting Information S1). Coverage is estimated as 85%. By increasing the pressure to 10 mN m^{-1}, the gap area was obviously dimin-
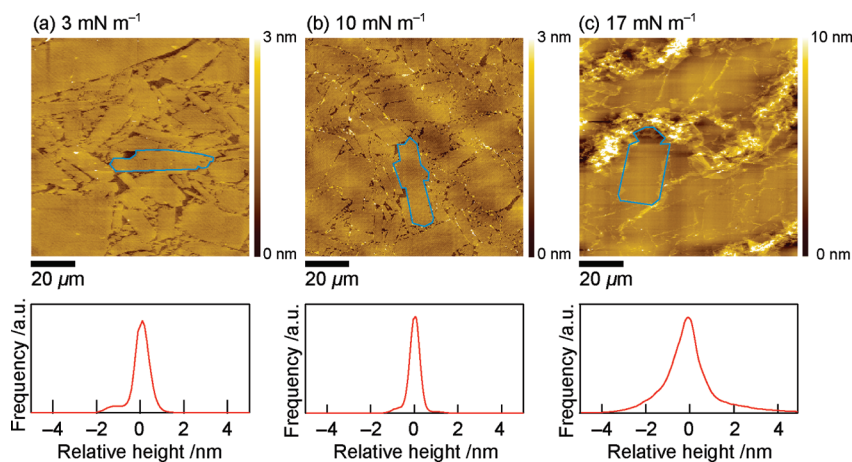
Figure 2. AFM images of $Ti_{0.87}O_2$ nanosheet films transferred onto silicon wafer at a surface pressure of (a) 3 mN m^{-1}, (b) 10 mN m^{-1}, and (c) 17 mN m^{-1}. The nanosheet concentration is 8 mg dm^{-3}. A selected nanosheet is outlined for clarity.

ished to yield 95% coverage (Figure 2b). The nanosheets with a lateral size of several tens of micrometers were densely packed, with their edges in contact basically side-by-side. The overlap between nanosheets was negligible at this pressure.[57] The film transferred at 15 mN m^{-1} showed a comparable neat texture except for overlapped patches starting to form in limited area (Supporting Information, Figure S2). In contrast, when the compression exceeded the inflection point of 16 mN m^{-1}, some nanosheets moved over neighboring sheets, yielding considerable overlap (Figure 2c and Supporting Information S2). The histogram shows a wider profile, reflecting the collapsed texture of the film. These results are consistent with compression−decompression behavior. The compression−decompression profile was nearly reversible when compression was set to achieve a pressure below 10 mN m^{-1} (Supporting Information, Figure S3a,b). Compression to a pressure of >16 mN m^{-1} resulted in irreversible behavior, suggesting the collapse of a monolayer of packed nanosheets. On the basis of the results above, surface compression to 10 mN m^{-1} and nanosheet concentration of 8 mg dm^{-3} were selected as the optimum condition for fabrication of well-organized films of the oversized titania nanosheets in this study.

Multilayer Buildup. Monolayer deposition involving surface compression to 10 mN m^{-1} was repeated to produce a multilayer film of the nanosheets. Exposure of the film to UV light after each LB transfer was essential for stable layer-by-layer growth into a multilayer structure. Without UV irradiation, film growth tended to slow down and eventually fail at some layer number. TBA ions are likely to cover the as-deposited film surface due to their interaction with the floating nanosheets at the air/liquid interface. We speculate that the hydrophobic nature of long alkyl chains is responsible for the failure of regular multilayer buildup. Exposure to UV light should promote photocatalytic de-
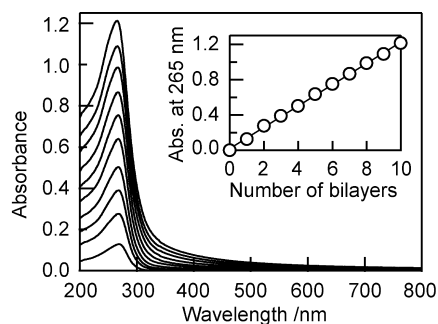
Figure 3. UV−visible absorption spectra in the layer-by-layer deposition process of the nanosheets on quartz glass substrate.

composition of TBA ions. Photocatalytic action was reported for titania nanosheets of $Ti_{0.87}O_2$ as well as $Ti_{0.91}O_2$.[58,59] UV irradiation for 2 min was enough to turn the surface hydrophilic.

Figure 3 displays UV−visible absorption spectra in the construction process of the multilayer film on the quartz glass substrate involving UV irradiation for 2 min between LB transfers. Nearly identical spectral evolution was observed in the deposition using prolonged UV-irradiation for 10 h, which was undertaken to ensure complete decomposition of TBA ions. The absorption band at 265 nm is attributable to $Ti_{0.87}O_2$ nanosheet, and its absorbance linearly increased by repeated deposition, indicating reproducible transfer of the well-organized monolayer of nanosheets. The average enhancement of absorbance at 265 nm was 0.12 per deposition of $Ti_{0.87}O_2$ monolayer on the both sides of the substrate. This absorbance gain is comparable to the previous data for multilayer films of titania nanosheets of $Ti_{0.91}O_2$ and $Ti_{0.87}O_2$ fabricated *via* sequential adsorption with polycation, for which substantial monolayer coverage in each deposition was confirmed.[35,46]

Furthermore, the highly organized texture of the film surface remained unchanged in the multilayer deposition, as revealed by AFM images for 5- and 10-layer films (Figure 4a,b), providing evidence for the re-
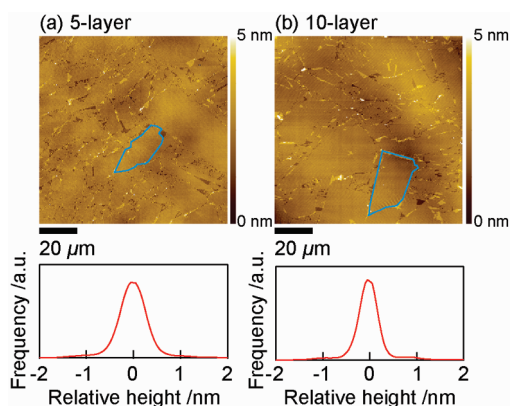
Figure 4. AFM images of $Ti_{0.87}O_2$ nanosheet films transferred onto silicon wafer at a surface pressure of 10 mN m^{-1}: (a) 5-layer, (b) 10-layer films.
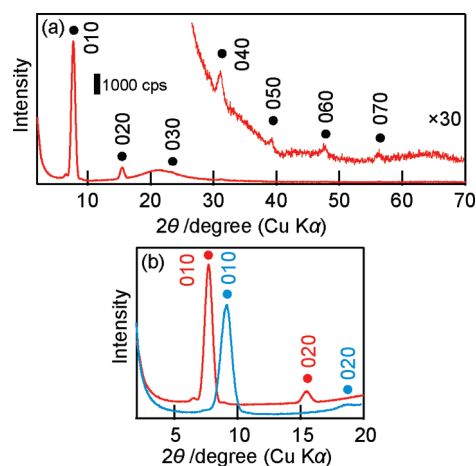
Figure 5. (a) XRD patterns for the 10-layer film of $Ti_{0.87}O_2$ nanosheet fabricated on the quartz glass; (b) expanded patterns. UV exposure time: 2 min (red), 10 h (blue).

peated deposition of well-packed nanosheets in the monolayer.

Figure 5a depicts XRD pattern for the 10-layer film of $Ti_{0.87}O_2$ nanosheet fabricated on the quartz glass. The film showed the 0k0 basal reflections up to the seventh order line,[60] indicating high structural order. The basal series can be ascribed to the stacked structure of the nanosheets. Figure 5b compares XRD data for 10-layer films of $Ti_{0.87}O_2$ nanosheets fabricated using different UV exposure time, 2 min and 10 h. The multilayer repeating distance was 1.14 and 0.94 nm, respectively, depending on the UV exposure time. The restacked structure of nanosheets accommodating TBA ions in the intersheet gallery can be synthesized as a powder form by freeze-drying the suspension.[61,62] Such materials have an interlayer distance of 1.75 nm, which is definitely larger than the values above. The shorter gallery height of the films in this study strongly suggests photocatalytic decomposition of TBA ions upon exposure to UV light in the deposition process, as expected. The multilayer spacing of 0.94 nm is identical to that for the UV-treated multilayer composite film of the smaller titania nanosheets, $Ti_{0.91}O_2$, and polycation, poly(diallyldimethylammonium) ion, fabricated *via* their sequential adsorption.[63] Such as-prepared film had a multilayer spacing of 1.5−1.7 nm.[35] UV irradiation brought about a gradual decrease in spacing to 0.94 nm. The final product was identified as an inorganic multilayer assembly accommodating NH_4^+, H^+, and H_2O as a consequence of total photocatalytic removal of organic polycations.[63] Since the oversized nanosheet of $Ti_{0.87}O_2$ in this study shows similar photocatalytic activity,[59] the multilayer film obtained *via* UV treatment for 10 h should be free from organic moieties. On the other hand, the relatively larger gallery height of 1.14 nm for the film prepared with 2 min of UV exposure may be reasonably explained by the presence of some partially decomposed product of TBA ions.
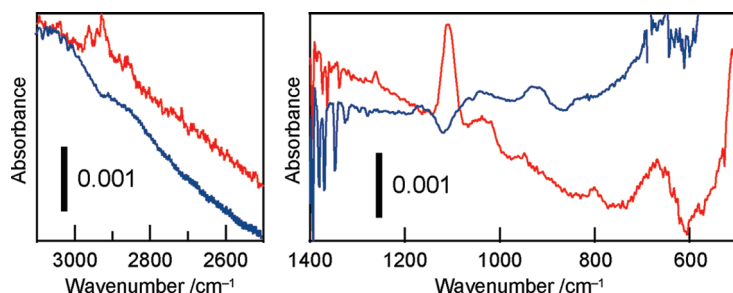
Figure 6. FT-IR spectra for the 10-layer film of $Ti_{0.87}O_2$ nanosheet fabricated on silicon wafer substrate. UV exposure time: 2 min (red), 10 h (blue).

Fourier transform infrared (FT-IR) spectra on these films confirm this explanation (Figure 6). The film fabricated *via* UV irradiation for 2 min showed noticeable absorption bands at wavenumbers of $3000-2800$ cm^{-1} and ~1100 cm^{-1}. The bands are attributable to stretching vibrations of CH_3 and CH_2 groups, and the $C-N$ bond, respectively, suggesting the presence of organic moieties in the film. It is to be pointed out that the relative intensity of the former bands with respect to the latter peak was much lower than that of the TBA ions,[64] suggesting the partial loss of alkyl chains. On the other hand, such bands were absent in the film fabricated *via* UV irradiation of 10 h. These results provide support for the partial and total decomposition of TBA ions for each film, which are introduced into the films during LB transfer.

Evaluation of Structural Order of the Films. One of the noticeable features in the XRD patterns of the films is the small satellite peaks around the 010 Bragg reflection (Figure 7a). The satellite peaks were more clearly observed for the film prepared *via* UV irradiation for 2 min. In the other film, they were poorly resolved and smeared out into a continuous skirt. The reason for this difference is not fully clear at the present stage. The complete removal of organic species may introduce slight structural disorder probably due to the direct geometrical contact and proximity of adjacent
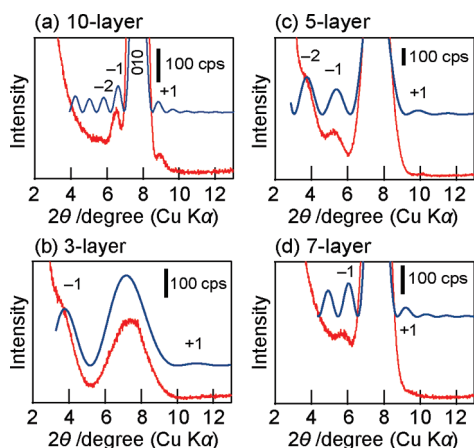

Figure 7. Enlarged view of XRD profile around 010 reflection for multilayer films of $Ti_{0.87}O_2$ nanosheet showing satellite peaks: (a) 10-, (b) 3-, (c) 5-, and (d) 7-layer films. Blue trace represents a calculated profile using eq 1.

nanosheets. In this study, we focus on the film showing clearer satellite peaks.

Interestingly, these satellites were present in films with a different number of LB cycles, and their relative position to the main peak was dependent on it, as shown in Figure 7b−d. These diffraction features suggest that the satellite peaks arise from the Laue interference function, which can be confirmed by the following calculation. XRD profile for a lamellar system composed of N stacked sheets can be given as

$$I(0k0) = \frac{1}{N} \cdot \frac{1 + \cos^2 2\theta}{\sin^2 \theta \cdot \cos \theta} \cdot \left| F(0k0) \right|^2 \cdot \frac{\sin^2(\pi Nk)}{\sin^2(\pi k)} \quad (1)$$

where the second term is the Lorentz-polarization factor, the third is the structure factor, and the fourth is the Laue interference function.[65,66] The structure factor is calculated on the basis of the atomic architecture of $Ti_{0.87}O_2$ nanosheet (see Supporting Information S4).[35] The simulated profiles basically match the observed pattern (Figure 7 blue line). A slight deviation from the ideal lattice may be responsible for the broader profile and invisible higher order ripples. Similar diffraction features arising from the interference function have been reported in artificial lattice films tailored by layer-by-layer construction involving vacuum deposition techniques, such as PLD and MBE. On the other hand, the appearance of Laue satellite peaks is very rare for films fabricated by wet-process deposition, apart from exceptional cases for LB films of amphiphilic molecules having long alkyl chains, such as stearic acids, which tend to organize into a well-ordered paraffin-type structure.[67,68]

Evolution of Laue satellite ripples as well as sharp basal peaks up to the seventh order definitely indicate very high structural order in the present LB films of $Ti_{0.87}O_2$ nanosheet. More explicitly, the number of nanosheet layers deposited is constant throughout the film, being identical to the number of LB transfers. Local fluctuation of the number of nanosheet layers should be negligible for the film size (in the order of centimeters). Cross-sectional TEM observations (Figure 8) provide direct information on the nanostructures. An image of the 10-layer film of $Ti_{0.87}O_2$ nanosheet deposited on the atomically flat substrate of $SrRuO_3$ revealed that the substrate surface is covered with the ultrathin film. The coverage and film thickness were homogeneous in a wide area. At a higher magnification, a lamellar fringe corresponding to the stacked nanosheets was clearly resolved.

As described above, XRD data indicate the formation of a highly ordered lamellar structure of the nanosheet. Thus, the XRD patterns are analyzed using

(a)

Nanosheet

Substrate

50 nm

(b)

N = 10

N = 2

N = 1

SrRuO$_3$
substrate
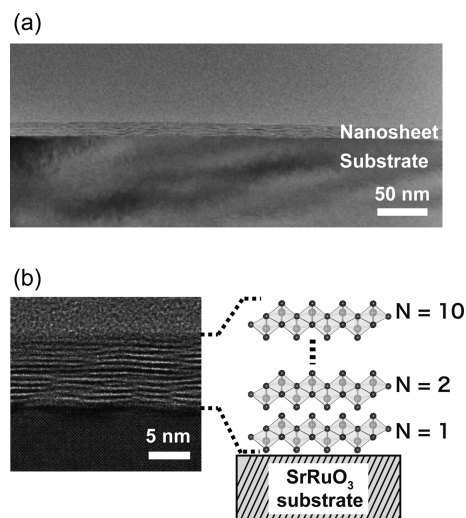
Figure 8. Cross-sectional TEM images of the 10 layer film of Ti$_{0.87}$O$_2$ nanosheet: (a) wide view; (b) magnified image.

the Williamson−Hall relationship,[69] given by eq 2, to quantitatively discuss the structural order.

$$\frac{\beta \cos \theta}{\lambda} = \frac{1}{\varepsilon} + 2\eta \frac{\sin \theta}{K\lambda} \qquad (2)$$

where β is fwhm *(full width at half maxima)* in radians, θ is the diffraction angle, ε is the crystallite size or coherent length in nm, η is the lattice strain, *K* is a shape correction factor taken as 0.9, and λ is the X-ray wavelength of the source (Cu Kα = 0.15405 nm). Here fwhm is corrected for instrumental broadening by applying the following equation.

$$\text{FWHM} = (\text{fwhm}_{sample}^2 - \text{fwhm}_{standard}^2)^{1/2} \qquad (3)$$

where fwhm$_{sample}$ and fwhm$_{standard}$ are a measured width at half-maximum of the diffraction peaks from the sample and the standard sample (1-tetradecanol was employed), respectively.

Figure 9 shows a plot of β cos θ/λ *versus* sin θ/λ for diffraction peaks from the 10-layer nanosheet film. The coherent length and strain were deduced from the intercept at the *y*-axis and the slope to be 11.8 nm and 0.08%, respectively. Because the multilayer repeated spacing is 1.14 nm, the thickness of the 10-layer film is
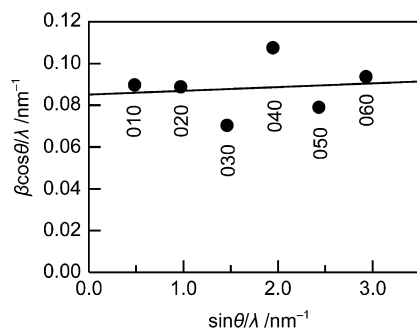
**Figure 9.** Williamson−Hall plot for the 10-layer film of Ti$_{0.87}$O$_2$ nanosheet.

TABLE 1. Crystallize-Size and Lattice Strain of Multilayer Films Fabricated by Various Procedures

procedure	sequential adsorption		Langmuir−Blodgett	
average nanosheet size	300 nm	10−30 μm	300 nm	10−30 μm
special treatment		ultrasonication		
strain (%)	10.96	0.62	4.20	0.08
crystallite size (nm)	3.3	8.5	6.9	11.8

expected to be 11.4 nm. The close similarity between this nominal film thickness and the coherent length obtained means that the X-ray is coherent for the whole film, again indicating the nearly perfect one-dimensional stacked structure of the nanosheets.[70] Furthermore, the extremely low value of lattice strain, 0.08%, should be noted as another measure for structural integrity. Artificial lattice films, such as GaAs, SiC, and ZnO, constructed by vapor-phase beam epitaxy techniques generally show lattice strain of 0.06−0.1%.[71−75]

As described in the first section, layer-by-layer assembled films of titania nanosheets with different lateral size were fabricated by sequential adsorption method and LB technique.[35,46,54] The film quality should be primarily dependent on the fabrication method and nanosheet size. Thus, it is of great interest to compare the structural order of the films fabricated by these two techniques using two different sizes of titania nanosheets such as Ti$_{0.87}$O$_2$ and Ti$_{0.91}$O$_2$. The former nanosheet, prepared from single crystals of K$_{0.8}$[Ti$_{1.73}$Li$_{0.27}$]O$_4$, is several tens of micrometers in size, and was used in the present study. On the other hand, the latter sheet is from a polycrystalline sample of Cs$_{0.7}$[Ti$_{1.825}$□$_{0.175}$]O$_4$ (□: vacancy) and is of submicrometers.[7,8] All the films showed basal diffraction peaks (Supporting Information S5) attributable to the layer-by-layer assembled nanosheets, but the line width reflecting the structural order differed for each one. Their profiles were analyzed by Williamson−Hall method and the results are summarized in Table 1. It is evident that the lateral size of nanosheets and the deposition procedure dominate the film quality. The LB method tends to yield films of higher quality in comparison with the sequential adsorption method. Larger nanosheets lead to higher structural order. Accordingly the film in the present study shows, by far, the best structural order among the four kinds of films.

Recently we found that well-organized films of titania nanosheets fabricated through sequential adsorption involving ultrasonic treatment exhibited excellent dielectric and insulating properties.[19,76] The 5−15 layer films gave a relative dielectric constant of ∼125, which is the highest among ultrathin films with a thickness of 10−20 nm of various high-*k* materials ((Ba,Sr)TiO$_3$, HfO$_2$, Ta$_2$O$_5$) investigated extensively.[77−81] The leakage current density for the 10-layer film was as low as 3.7 × 10^{-9} A cm^{-2} at 1 V, again being much superior to the
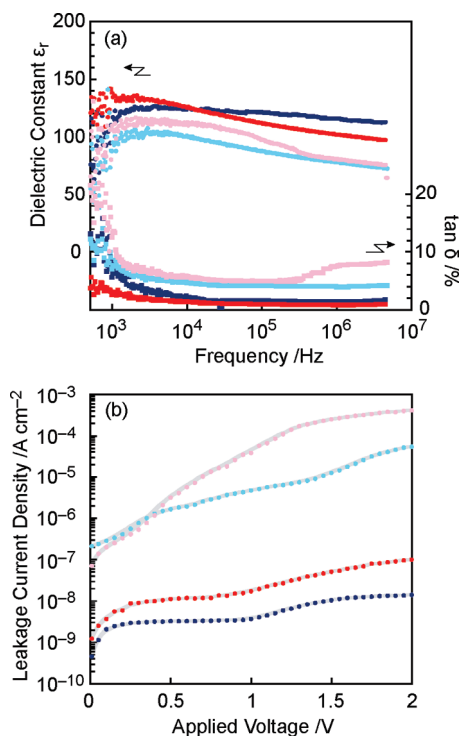
Figure 10. (a) Frequency dependence of relative dielectric constant ε_r and the dielectric loss $\tan \delta$, and leakage current density versus voltage ($J-V$) curves for the 10-layer films of large-sized $Ti_{0.87}O_2$ and small-sized $Ti_{0.91}O_2$ nanosheets: (red) $Ti_{0.87}O_2$ by LB deposition; (blue) $Ti_{0.87}O_2$ by sequential adsorption involving ultrasonication; (aqua) $Ti_{0.91}O_2$ by LB deposition; (pink) $Ti_{0.91}O_2$ by sequential adsorption.

comparable films of other high-*k* materials. As described above, we have four kinds of titania nanosheet films in various quality. Thus, it is interesting to examine how the film architecture affects the electric properties. As depicted in Figure 10, the films of small-sized

nanosheet of $Ti_{0.91}O_2$, either fabricated through sequential adsorption or LB method, did not show satisfactory dielectric performance and insulating properties. Leakage current density of such films was higher by several orders of magnitude than that for the other two films. This poor insulating behavior should be due to the rather disorganized film architecture having pinholes and voids and is responsible for failure in realizing high dielectric performance. On the other hand, the leakage current density for the LB film of $Ti_{0.87}O_2$ nanosheet was low enough to provide the dielectric performance intrinsic to the nanosheet. The obtained relative dielectric constant of 125 was comparable to that attained with the $Ti_{0.87}O_2$ nanosheet film by sequential adsorption and ultrasonication. Somewhat larger leakage current may be associated with the fact that the LB film tends to have a gap rather than an overlap while *vice versa* for the film *via* sequential adsorption route.

CONCLUSIONS

We have demonstrated for the first time successful fabrication of highly organized monolayer and multilayer films composed of large-sized titania nanosheets by LB deposition procedure. The air/liquid interface where nanosheets several tens of micrometers in size spontaneously float was compressed to an optimized surface pressure and the resulting film of nanosheets was transferred onto the substrate. AFM observations confirmed that the sheets were well-packed with negligible overlapped patches and gaps. Repetition of this monolayer deposition led to the highly ordered multilayer structure of the stacked nanosheets. The structural integrity was comparable to that for films of artificial lattice produced by advanced vacuum deposition techniques.

EXPERIMENTAL SECTION

Reagents and Materials. Reagents such as TiO_2, K_2CO_3, Li_2CO_3, and MoO_3 (Rare Metallic) were of >99.9% purity. Other chemicals used were of analytical grade. Ultrapure water (>18 MΩ cm) obtained with a Milli-Q filtration system was used throughout the experiments. A colloidal suspension of $Ti_{0.87}O_2$ nanosheet was synthesized according to a previously reported procedure.[45] A single crystal of layered titanate of $K_{0.8}[Ti_{1.73}Li_{0.27}]O_4$ was prepared by slowly cooling a flux melt of MoO_3 containing a mixture of TiO_2, K_2CO_3, and Li_2CO_3 from 1200 to 950 °C at a rate of 4 °C h^{-1}. The obtained single crystal was converted into a protonic oxide of $H_{1.07}Ti_{1.73}O_4 \cdot H_2O$ by repeated acid exchange using a 0.5 mol dm^{-3} HCl aqueous solution (24 h × 5). The protonic oxide was washed with copious amounts of water, air-dried, and then allowed to react with an aqueous solution of 2.4 mmol dm^{-3} TBA hydroxide. The solution-to-solid ratio was 250 cm^3 g^{-1} and the mixture was shaken gently for 3 weeks, which produced the colloidal suspension of monodispersed and unilamellar $Ti_{0.87}O_2$ nanosheet. AFM observations indicated that the sheets were 10−30 μm in lateral size and 1.2−1.3 nm in thickness (Supporting Information S1).

Fabrication of Multilayer Films. Silicon wafer and quartz glass substrates were cleaned by treatment with HCl/CH$_3$OH solution (HCl/CH$_3$OH = 1:1 v/v) and then concentrated H$_2$SO$_4$ for 30 min each, while SrRuO$_3$ substrates with atomically flat surface were

photochemically cleaned by irradiation of UV light in ozone atmosphere. Film fabrication was carried out using a USI FSD-3-777 double barrier Langmuir trough (Teflon coating, active trough surface area 34.4 × 10 cm^2, trough volume 250 cm^3) equipped with a Wilhelmy-type balance for surface pressure measurement. The typical procedure for LB deposition is as follows. The colloidal suspension of $Ti_{0.87}O_2$ nanosheet was diluted with ultrapure water to a concentration of 8 mg dm^{-3}, and was placed in the LB trough at a regulated temperature of 25 ± 0.5 °C. After 20 min, the surface of the suspension started to compress at a rate of 0.5 mm s^{-1} until the surface pressure reached 10 mN m^{-1}. After maintaining a constant pressure for 20 min, the film at the interface was transferred onto the substrate using the vertical dipping method at a transfer rate of 1.0 mm min^{-1}. Then, the substrate was dried at 110 °C for 20 min, and exposed to UV light (<300 nm) with a light intensity of 1 mW cm^{-2} for 2 min. These operations were repeated *n* times to synthesize a multilayer film of $Ti_{0.87}O_2$ nanosheet.

Measurements. XRD patterns were collected by a powder diffractometer (Rigaku Rint 2100) with monochromatized Cu Kα radiation (λ = 0.15405 nm). UV−visible absorption spectra of the multilayer films on quartz glass substrate were recorded on a Hitachi U-4100 UV−visible spectrophotometer. FT-IR spectra of the films on silicon wafer were acquired in transmission mode using Varian 7000e FT-IR spectrophotometer. AFM images of the

mono- and multilayer films were obtained with an SPA 400 (Seiko Instruments) system in tapping mode using silicon probes with a force constant of 20 N m^{-1}. All images were taken in ambient atmosphere. Cross-sectional TEM observations were carried out using a Hitachi H-9000 microscope operating at 200 kV, which has a point resolution of 0.1 nm. TEM specimens were prepared by Ar ion milling after molding in epoxy glue. Electric measurements were carried out for the films fabricated on SrRuO$_3$ substrate as a bottom electrode by depositing Au top electrodes. An Agilent Technologies 4294A precision impedance analyzer was used to obtain capacitance and dielectric loss, and a Keithley 4200-SCS semiconductor parameter analyzer was employed to measure leakage current densities.

Supporting Information Available: Structure of Ti$_{0.87}$O$_2$ nanosheet, AFM images of the nanosheet films fabricated at various conditions, hysteresis $\pi-A$ behavior of Ti$_{0.87}$O$_2$ nanosheet at the air/water interface, method for calculating the structure factor, and XRD patterns of 10-layer nanosheet films synthesized by various assembly techniques. This material is available free of charge *via* the Internet at http://pubs.acs.org.

REFERENCES AND NOTES

1. Rao, S. G.; Huang, L.; Setyawan, W.; Hong, S. Large-Scale Assembly of Carbon Nanotubes. *Nature* **2003**, *425*, 36–37.
2. Shevchenko, E. V.; Kotov, N. A.; O'Brien, S.; Talapin, D. V.; Murray, C. B. Structural Diversity in Binary Nanoparticle Superlattices. *Nature* **2006**, *439*, 55–59.
3. Chang, S.; Shih, C.; Chen, C.; Lai, W.; Wang, C. R. C. The Shape Transition of Gold Nanorods. *Langmuir* **1999**, *15*, 701–709.
4. Korgel, B. A.; Fitzmaurice, D. Self-Assembly of Silver Nanocrystals into Two-Dimensional Nanowire Arrays. *Adv. Mater.* **1998**, *10*, 661–665.
5. Li, M.; Schnablegger, H.; Mann, S. Coupled Synthesis and Self-Assembly of Nanoparticles to Give Structures with Controlled Organization. *Nature* **1999**, *402*, 393–395.
6. Decher, G. Fuzzy Nanoassemblies: Toward Layered Polymeric Multicomposites. *Science* **1997**, *277*, 1232–1237.
7. Sasaki, T.; Watanabe, M.; Hashizume, H.; Yamada, H.; Nakazawa, H. Macromolecule-like Aspects for a Colloidal Suspension of an Exfoliated Titanate. Pairwise Association of Nanosheets and Dynamic Reassembling Process Initiated from It. *J. Am. Chem. Soc.* **1996**, *118*, 8329–8335.
8. Sasaki, T.; Watanabe, M. Osmotic Swelling to Exfoliation. Exceptionally High Degrees of Hydration of a Layered Titanate. *J. Am. Chem. Soc.* **1998**, *120*, 4682–4689.
9. Omomo, Y.; Sasaki, T.; Wang, L. Z.; Watanabe, M. Redoxable Nanosheet Crystallites of MnO$_2$ Derived *via* Delamination of a Layered Manganese Oxide. *J. Am. Chem. Soc.* **2003**, *125*, 3568–3575.
10. Ebina, Y.; Sasaki, T.; Watanabe, M. Study on Exfoliation of Layered Perovskite-Type Niobates. *Solid State Ionics* **2002**, *151*, 177–182.
11. Nadeau, P. H.; Wilson, M. J.; McHardy, W. J.; Tait, J. M. Interstratified Clays as Fundamental Particles. *Science* **1984**, *225*, 923–925.
12. Fang, M.; Kim, C. H.; Saupe, G. B.; Kim, H.-N.; Waraksa, C. C.; Miwa, T.; Fujishima, A.; Mallouk, T. E. Layer-by-Layer Growth and Condensation Reactions of Niobate and Titanoniobate Thin Films. *Chem. Mater.* **1999**, *11*, 1526–1532.
13. Fukuda, K.; Nakai, I.; Ebina, Y.; Ma, R.; Sasaki, T. Colloidal Unilamellar Layers of Tantalum Oxide with Open Channels. *Inorg. Chem.* **2007**, *46*, 4787–4789.
14. Takagaki, A.; Lu, D.; Kondo, J. N.; Hara, M.; Hayashi, S.; Domen, K. Exfoliated HNb$_3$O$_8$ Nanosheets as a Strong Protonic Solid Acid. *Chem. Mater.* **2005**, *17*, 2487–2489.
15. Miyamoto, N.; Yamamoto, H.; Kaito, R.; Kuroda, K. Formation of Extraordinarily Large Nanosheets from K$_4$Nb$_6$O$_{17}$ Crystals. *Chem. Commun.* **2002**, 2378–2379.
16. Sugimoto, W.; Terabayashi, O.; Murakami, Y.; Takasu, Y. Electrophoretic Deposition of Negatively Charged Tetratitanate Nanosheets and Transformation into Preferentially Oriented TiO$_2$(B) Film. *J. Mater. Chem.* **2002**, *12*, 3814–3818.
17. Geim, A. K.; Novoselov, K. S. The Rise of Graphene. *Nat. Mater.* **2007**, *6*, 183–191.
18. Sakai, N.; Ebina, Y.; Takada, K.; Sasaki, T. Electronic Band Structure of Titania Semiconductor Nanosheets Revealed by Electrochemical and Photoelectrochemical Studies. *J. Am. Chem. Soc.* **2004**, *126*, 5851–5858.
19. Osada, M.; Ebina, Y.; Funakubo, H.; Yokoyama, S.; Kiguchi, T.; Takada, K.; Sasaki, T. High-*k* Dielectric Nanofilms Fabricated from Titania Nanosheets. *Adv. Mater.* **2006**, *18*, 1023–1027.
20. Osada, M.; Ebina, Y.; Takada, K.; Sasaki, T. Gigantic Magneto-Optical Effects in Multilayer Assemblies of Two-Dimensional Titania Nanosheets. *Adv. Mater.* **2006**, *18*, 295–299.
21. Osada, M.; Ebina, Y.; Fukuda, K.; Ono, K.; Takada, K.; Yamaura, K.; Takayama-Muromachi, E.; Sasaki, T. Ferromagnetism in Two-Dimensional Ti$_{0.8}$Co$_{0.2}$O$_2$ Nanosheets. *Phys. Rev. B* **2006**, *73*, 153301.
22. Osada, M.; Itose, M.; Ebina, Y.; Ono, K.; Ueda, S.; Kobayashi, K.; Sasaki, T. Gigantic Magneto-Optical Effects Induced by (Fe/Co)-Cosubstitution in Titania Nanosheets. *Appl. Phys. Lett.* **2008**, *92*, 253110−1253110−3.
23. Ida, S.; Ogata, C.; Unal, U.; Izawa, K.; Inoue, T.; Altuntasoglu, O.; Matsumoto, Y. Preparation of a Blue Luminescent Nanosheet Derived from Layered Perovskite Bi$_2$SrTa$_2$O$_9$. *J. Am. Chem. Soc.* **2007**, *129*, 8956–8957.
24. Ozawa, T. C.; Fukuda, K.; Akatsuka, K.; Ebina, Y.; Sasaki, T. Preparation and Characterization of the Eu^{3+} Doped Perovskite Nanosheet Phosphor: La$_{0.90}$Eu$_{0.05}$Nb$_2$O$_7$. *Chem. Mater.* **2007**, *19*, 6575–6780.
25. Ozawa, T. C.; Fukuda, K.; Akatsuka, K.; Ebina, Y.; Sasaki, T. Eu$_{0.56}$Ta$_2$O$_7$: A New Nanosheet Phosphor with the High Intrananosheet Site Photoactivator Concentration. *J. Phys. Chem. C* **2008**, *112*, 1312–1315.
26. Ozawa, T. C.; Fukuda, K.; Akatsuka, K.; Ebina, Y.; Sasaki, T.; Kurashima, K.; Kosuda, K. (K$_{1.5}$Eu$_{0.5}$)Ta$_3$O$_{10}$: A Far-Red Luminescent Nanosheet Phosphor with the Double Perovskite Structure. *J. Phys. Chem. C* **2008**, *112*, 17115–17120.
27. Ida, S.; Ogata, C.; Eguchi, M.; Youngblood, W. J.; Mallouk, T. E.; Matsumoto, Y. Photoluminescence of Perovskite Nanosheets Prepared by Exfoliation of Layered Oxides, K$_2$Ln$_2$Ti$_3$O$_{10}$, KLnNb$_2$O$_7$, and RbLnTa$_2$O$_7$ (Ln: Lanthanide Ion). *J. Am. Chem. Soc.* **2008**, *130*, 7052–7059.
28. Ida, S.; Ogata, C.; Shiga, D.; Izawa, K.; Ikeue, K.; Matsumoto, Y. Dynamic Control of Photoluminescence for Self-Assembled Nanosheet Films Intercalated with Lanthanide Ions by Using a Photoelectrochemical Reaction. *Angew. Chem., Int. Ed.* **2008**, *47*, 2480–2483.
29. Sakai, N.; Fukuda, K.; Omomo, Y.; Ebina, Y.; Takada, K.; Sasaki, T. Hetero-Nanostructured Films of Titanium and Manganese Oxide Nanosheets: Photoinduced Charge Transfer and Electrochemical Properties. *J. Phys. Chem. C* **2008**, *112*, 5197–5202.
30. Fukuda, K.; Akatsuka, K.; Ebina, Y.; Ma, R.; Takada, K.; Nakai, I.; Sasaki, T. Exfoliated Nanosheet Crystallite of Cesium Tungstate with 2D Pyrochlore Structure: Synthesis, Characterization, and Photochromic Properties. *ACS Nano* **2008**, *2*, 1689–1695.
31. Keller, S. W.; Kim, H.-N.; Mallouk, T. E. Layer-by-Layer Assembly of Intercalation Compounds and Heterostructures on Surfaces: Toward Molecular Beaker Epitaxy. *J. Am. Chem. Soc.* **1994**, *116*, 8817–8818.
32. Kotov, N. A.; Dékány, I.; Fendler, J. H. Ultrathin Graphite Oxide−Polyelectrolyte Composites Prepared by Self-Assembly: Transition Between Conductive and Non-conductive States. *Adv. Mater.* **1996**, *8*, 637–641.

33. Fang, M.-M.; Kaschak, D. M.; Sutorik, A. C.; Mallouk, T. E. A "Mix and Match" Ionic−Covalent Strategy for Self-Assembly of Inorganic Multilayer Films. *J. Am. Chem. Soc.* **1997**, *119*, 12184−12191.

34. Kim, H.-N.; Keller, S. W.; Mallouk, T. E.; Schmitt, J.; Decher, G. Characterization of Zirconium Phosphate/Polycation Thin Films Grown by Sequential Adsorption Reactions. *Chem. Mater.* **1997**, *9*, 1414−1421.

35. Sasaki, T.; Ebina, Y.; Tanaka, T.; Harada, M.; Watanabe, M. Layer-by-Layer Assembly of Titania Nanosheet/Polycation Composite Films. *Chem. Mater.* **2001**, *13*, 4661−4667.

36. Schaak, R. E.; Mallouk, T. E. Perovskites by Design: A Toolbox of Solid-State Reactions. *Chem. Mater.* **2002**, *14*, 1455−1471.

37. Wang, L. Z.; Omomo, Y.; Sakai, N.; Fukuda, K.; Nakai, I.; Ebina, Y.; Takada, K.; Watanabe, M.; Sasaki, T. Fabrication and Characterization of Multilayer Ultrathin Films of Exfoliated MnO_2 Nanosheets and Polycations. *Chem. Mater.* **2003**, *15*, 2873−2878.

38. Yui, T.; Tsuchino, T.; Itoh, T.; Ogawa, M.; Fukushima, Y.; Takagi, K. Photoinduced One-Electron Reduction of MV^{2+} in Titania Nanosheets Using Porphyrin in Mesoporous Silica Thin Films. *Langmuir* **2005**, *21*, 2644−2646.

39. Sakai, N.; Ebina, Y.; Takada, K.; Sasaki, T. Photocurrent Generation from Semiconducting Manganese Oxide Nanosheets in Response to Visible Light. *J. Phys. Chem. B* **2005**, *109*, 9651−9655.

40. Yui, T.; Tsuchino, T.; Akatsuka, K.; Yamauchi, A.; Kobayashi, Y.; Hattori, T.; Haga, M.; Takagi, K. Visible Light-Induced Electron Transfers in Titania Nanosheet and Mesoporous Silica Integrated Films. *Bull. Chem. Soc. Jpn.* **2006**, *79*, 386−396.

41. Akatsuka, K.; Ebina, Y.; Muramatsu, M.; Sato, T.; Hester, H.; Kumaresan, D.; Schmehl, R. H.; Sasaki, T.; Haga, M. Photoelectrochemical Properties of Alternating Multilayer Films Composed of Titania Nanosheets and Zn Porphyrin. *Langmuir* **2007**, *23*, 6730−6736.

42. Kim, T. W.; Hur, S. G.; Hwang, S.-J.; Park, H.; Choi, W.; Choy, J.-H. Heterostructured Visible-Light-Active Photocatalyst of Chromia-Nanoparticle-Layered Titanate. *Adv. Funct. Mater.* **2007**, *17*, 307−314.

43. Mallouk, T. E.; Gavin, J. A. Molecular Recognition in Lamellar Solids and Thin Films. *Acc. Chem. Res.* **1998**, *31*, 209−217.

44. Shibata, T.; Fukuda, K.; Ebina, Y.; Kogure, T.; Sasaki, T. One-Nanometer-Thick Seed Layer of Unilamellar Nanosheets Promotes Oriented Growth of Oxide Crystal Films. *Adv. Mater.* **2008**, *20*, 231−235.

45. Tanaka, T.; Ebina, Y.; Takada, K.; Kurashima, K.; Sasaki, T. Oversized Titania Nanosheet Crystallites Derived from Flux-Grown Layered Titanate Single Crystals. *Chem. Mater.* **2003**, *15*, 3564−3568.

46. Tanaka, T.; Fukuda, K.; Ebina, Y.; Takada, K.; Sasaki, T. Highly Organized Self-Assembled Monolayer and Multilayer Films of Titania Nanosheets. *Adv. Mater.* **2004**, *16*, 872−875.

47. Inukai, K.; Hotta, Y.; Taniguchi, M.; Tomura, S.; Yamagishi, A. Formation of a Clay Monolayer at an Air−Water Interface. *J. Chem. Soc., Chem. Commun.* **1994**, 959.

48. Kotov, N. A.; Meldrum, F. C.; Fendler, J. H.; Tombácz, E.; Dèkány, I. Spreading of Clay Organocomplexes on Aqueous Solutions: Co�nstruction of Langmuir-Blodgett Clay Organocomplex Multilayer Films. *Langmuir* **1994**, *10*, 3797−3804.

49. Tamura, K.; Setsuda, H.; Taniguchi, M.; Nakamura, T.; Yamagishi, A. A Clay−Metal Complex Ultrathin Film as Prepared by the Langmuir-Blodgett Technique. *Chem. Lett.* **1999**, *28*, 121−122.

50. Taguchi, Y.; Kimura, R.; Azumi, R.; Tachibana, H.; Koshizaki, N.; Shimomura, M.; Momozawa, N.; Sakai, H.; Abe, M.; Matsumoto, M. Fabrication of Hybrid Layered Films of MoS_2 and an Amphiphilic Ammonium Cation Using the Langmuir−Blodgett Technique. *Langmuir* **1998**, *14*, 6550−6555.

51. Yamaki, T.; Asai, K. Alternate Multilayer Deposition from Ammonium Amphiphiles and Titanium Dioxide Crystalline Nanosheets Using the Langmuir−Blodgett Technique. *Langmuir* **2001**, *17*, 2564−2567.

52. Umemura, Y.; Yamagishi, A.; Schoonheydt, R.; Persoons, A.; De Schryver, F. Langmuir−Blodgett Films of a Clay Mineral and Ruthenium(II) Complexes with a Noncentrosymmetric Structure. *J. Am. Chem. Soc.* **2002**, *124*, 992−997.

53. Ras, R. H. A.; Johnston, C. T.; Franses, E. I.; Ramaekers, R.; Maes, G.; Foubert, P.; De Schryver, F. C.; Schoonheydt, R. A. Polarized Infrared Study of Hybrid Langmuir−Blodgett Monolayers Containing Clay Mineral Nanoparticles. *Langmuir* **2003**, *19*, 4295−4302.

54. Muramatsu, M.; Akatsuka, K.; Ebina, Y.; Wang, K.; Sasaki, T.; Ishida, T.; Miyake, K.; Haga, M. Fabrication of Densely Packed Titania Nanosheet Films on Solid Surface by Use of Langmuir−Blodgett Deposition Method without Amphiphilic Additives. *Langmuir* **2005**, *21*, 6590−6595.

55. Kawamata, J.; Seike, R.; Higashi, T.; Inada, Y.; Ogata, Y.; Tani, S.; Yamagishi, A. Clay Templating Langmuir−Blodgett Films of a Nonamphiphilic Ruthenium(II) Complex. *Colloids Surf., A* **2006**, *284*, 135−139.

56. The abundance of floating nanosheets can be estimated by the area between the sliding barriers where a rise of surface pressure is observed.

57. The similar well-organized texture was obtained from the suspension with lower concentrations of 2 and 4 mg dm^{-3} (Supporting Information S2a) although a larger degree of trough-area compression was needed. On the other hand, the film from the suspension of 12 mg dm^{-3} did not have the neat-tiling of the nanosheets and gaps were formed between the nanosheets (Supporting Information S2b). TBA ions may be present in the gap because of their higher concentration.

58. Sakai, N.; Fukuda, K.; Shibata, T.; Ebina, Y.; Takada, K.; Sasaki, T. Photoinduced Hydrophilic Conversion Properties of Titania Nanosheets. *J. Phys. Chem. B* **2006**, *110*, 6198−6203.

59. Shibata, T.; Sakai, N.; Fukuda, K.; Ebina, Y.; Sasaki, T. Photocatalytic Properties of Titania Nanostructured Films Fabricated from Titania Nanosheets. *Phys. Chem. Chem. Phys.* **2007**, *9*, 2413−2420.

60. The *a*- and *c*-axes are taken in parallel to the 2D nanosheet plane according to the orthorhombic structure of the starting titanate, $K_{0.8}[Ti_{1.73}Li_{0.27}]O_4$.

61. Sasaki, T.; Nakano, S.; Yamauchi, S.; Watanabe, M. Fabrication of Titanium Dioxide Thin Flakes and Their Porous Aggregate. *Chem. Mater.* **1997**, *9*, 602−608.

62. Iida, M.; Sasaki, T.; Watanabe, M. Titanium Dioxide Hollow Microspheres with an Extremely Thin Shell. *Chem. Mater.* **1998**, *10*, 3780−3782.

63. Sasaki, T.; Ebina, Y.; Fukuda, K.; Tanaka, T.; Harada, M.; Watanabe, M. Titania Nanostructured Films Derived from a Titania Nanosheet/Polycation Multilayer Assembly *via* Heat Treatment and UV Irradiation. *Chem. Mater.* **2002**, *14*, 3524−3530.

64. Abs. (@2920 cm^{-1})/Abs. (@1109 cm^{-1}) = 0.1 for the film while it is 2 for TBA^+Br^- (Aldrich FT-IR Library).

65. Reynolds, R. C., Jr. *Modern Powder Diffraction*; Bish, D. L., Post, J. E., Eds.; The Mineralogical Society of America: Washington, DC, 1989; pp 159.

66. Sasaki, T.; Ebina, Y.; Watanabe, M.; Decher, G. Multilayer Ultrathin Films of Molecular Titania Nanosheets Showing Highly Efficient UV-Light Absorption. *Chem. Commun.* **2000**, 2163−2164.

67. Frieling, M. V.; Bradaczek, H.; Durfee, W. S. X-ray Diffraction of Langmuir−Blodgett Films: Establishing a New Method for the Calculation of Electron-Density Distributions from a Single Set of Intensity Data. *Thin Solid Films* **1988**, *159*, 451−459.

68. Pomerantz, M.; Segmüller, A. High-Resolution X-ray Diffraction from Small Numbers of Langmuir−Blodgett Layers of Manganese Stearate. *Thin Solid Films* **1980**, *68*, 33−45.

69. Williamson, G. K.; Hall, W. H. X-ray Line Broadening from Filed Aluminum and Wolfram. *Acta Metal.* **1953**, *1*, 22–31.

70. Due to the nature of synthetic process, the lateral alignment of the nanosheets in the film was not able to be controlled. Thus the film architecture is described as the one-dimensional stacked structure.

71. Chizmeshya, A. V. G.; Ritter, C. J.; Hu, C.; Tice, J. B.; Tolle, J.; Nieman, R. A.; Tsong, I. S. T.; Kouvetakis, J. Synthesis of Butane-like SiGe Hydrides: Enabling Precursors for CVD of Ge-Rich Semiconductors. *J. Am. Chem. Soc.* **2006**, *128*, 6919–6930.

72. Tan, S. T.; Chen, B. J.; Sun, X. W.; Fan, W. J.; Kwok, H. S.; Zhang, X. H.; Chua, S. J. Blueshift of Optical Band Gap in ZnO Thin Films Grown by Metal−Organic Chemical-Vapor Deposition. *J. Appl. Phys.* **2005**, *98*, 013505.

73. Vailionis, A.; Brazdeikis, A.; Flodström, A. S. Microstructural Properties of $Bi_2Sr_2Ca_{n-1}Cu_nO_y$ Multilayers Grown by Molecular Beam Epitaxy. *Phys. Rev. B* **1996**, *54*, 15457–15462.

74. Tabata, H.; Kawai, T. Dielectric Properties of Strained (Sr, Ca)TiO_3/(Ba, Sr)TiO_3 Artificial Lattices. *Appl. Phys. Lett.* **1997**, *70*, 321–323.

75. Nomura, I.; Yamazaki, T.; Hayashi, H.; Hayami, K.; Kato, M.; Kishino, K. Zn Irradiation Effects in MBE Growth of MgSe/BeZnSeTe II−VI Compound Superlattices on InP Substrates. *J. Cryst. Growth* **2007**, *301*, 273–276.

76. Osada, M.; Akatsuka, K.; Ebina, Y.; Kotani, Y.; Ono, K.; Funakubo, H.; Ueda, S.; Kobayashi, K.; Takada, K.; Sasaki, T. Langmuir−Blodgett Fabrication of Nanosheet-Based Dielectric Films without an Interfacial Dead Layer. *Jpn. J. Appl. Phys.* **2008**, *47*, 7556–7560.

77. Kingon, A. I.; Maria, J.-P.; Streiffer, S. K. Alternative Dielectrics to Silicon Dioxide for Memory and Logic Devices. *Nature* **2000**, *406*, 1032–1038.

78. Kim, S. K.; Kim, W.-D.; Kim, K.-M.; Hwang, C. S.; Jeong, J. High Dielectric Constant TiO_2 Thin Films on a Ru Electrode Grown at 250°C by Atomic-Layer Deposition. *Appl. Phys. Lett.* **2004**, *85*, 4112–4114.

79. Hwang, C. S.; Park, S. O.; Cho, H.-J.; Kang, C. S.; Kang, H. K.; Lee, S. I.; Lee, M. Y. Deposition of Extremely Thin (Ba, Sr)TiO_3 Thin Films for Ultra-Large-Scale Integrated Dynamic Random-Access Memory Application. *Appl. Phys. Lett.* **1995**, *67*, 2819–2821.

80. Werner, M. C.; Banerjee, I.; McIntyre, P. C.; Tani, N.; Tanimura, M. Microstructure of (Ba, Sr)TiO_3 Thin Films Deposited by Physical Vapor Deposition at 480°C and Its Influence on the Dielectric Properties. *Appl. Phys. Lett.* **2000**, *77*, 1209–1211.

81. Hwang, C. S. Thickness-Dependent Dielectric Constants of (Ba, Sr)TiO_3 Thin Films with Pt or Conducting Oxide Electrodes. *J. Appl. Phys.* **2002**, *92*, 432–437.